Scholar Publishing Group
International Journal of Big Data Intelligent Technology
https://doi.org/10.38007/IJBDIT.2020.010205
ISSN 2790-0932 Vol. 1, Issue 2: 58-73

Image Distortion When Detecting Nano-Scale Ferroelectric Domains with Piezoelectric Force Microscope Based on Depth Image Segmentation

Ramyan Radhakrishnan*

Jimma University, Ethiopia

**corresponding author*

Keywords: Image Segmentation, Ferroelectric Domain Structure, Piezoelectric Force Microscope, Image Distortion

Abstract: The research on the microstructure and properties of ferroelectric materials has attracted more and more attention. This article aims to study the nanoscale microscopic images of ferroelectric domains through piezoelectric force microscope. This paper proposes the method of deep image cutting to obtain microscopic images of ferroelectric domains, so as to study the nano-scale three-dimensional domain structure imaging of specific regions of ferroelectric domains, and control the operation of the domain structure and the dynamic study under the action of external fields. Imaging and quantitative characterization of physical properties such as ferroelectricity and piezoelectricity. Then use the image segmentation technology to obtain the image of the ferroelectric domain structure we want. This paper investigates the image distortion problem when the piezoelectric force microscope of depth image segmentation detects nano-scale ferroelectric domains, finds the key factors of image distortion, and reduces the probability of image distortion by 20%.

1 Introduction

With the continuous development of science and technology in the micro and nano fields, micro and nano materials and their manufacturing have been more and more widely used in high-tech fields such as chip manufacturing, electronic packaging, and biomedicine. 2006-2020)" has listed micro and nano materials, micro-nano system manufacturing, and ultra-precision processing as key research content. In the field of micro-nano system manufacturing, ultra-precision processing technology has developed rapidly, and various micro-mechanical systems and MEMS (micro-electromechanical systems) devices have appeared. These micro-nano devices or systems are usually composed of a variety of micro- and nano-materials. The elastic modulus and thermal

expansion coefficient of the materials are different. Under different load, humidity and temperature conditions, micro-cracks are prone to occur at the junctions of the materials, leading to failure of the micro-nano devices. Therefore, the implementation of accurate three-dimensional surface measurement at the micro-nano scale is of great significance for understanding the deformation mechanism of micro-nano materials, guiding the design of micro-nano devices and manufacturing of micro-nano systems, and analyzing their failure mechanisms. Image processing technology involves various fields of computer science, such as artificial intelligence, computer vision, medical imaging, etc. The maturity of image processing technology is directly related to the development of its related fields, and it is necessary to study image processing technology. Image segmentation is the prerequisite for the study of image processing technology, which has a direct impact on the subsequent processing of images, and has always attracted the attention of the scientific community.

For the imaging of nanostructures of ferroelectric domains, experts and scholars at home and abroad have already carried out many researches in this area. Lambeck PV studied the development of this stability in a Mn-doped BaTiO 3 single crystal with a special domain structure. It is concluded that the considerable stability in this material is due to the volume effect, which means that the gradual reorientation of the polar defects with respect to the direction of spontaneous polarization, there is no 180 ° domain wall pinning and surface layer effects at all. [1]. Katayama K studied the orientation control of {100} orientation epitaxial orthogonal 0.07YO1.5-0.93HfO2 thin films grown by pulsed laser deposition. The current results show that the orientation of HfO2-based ferroelectric films can be controlled in the same way as ferroelectric films composed of conventional perovskite-type materials such as Pb(Zr, Ti)O3 and BiFeO3 [2]. In order to stabilize the perovskite structure and increase the storage energy density (U) of Pb(Tm1/2Nb1/2)O3 (PTmN)-based materials, Wang Z introduced Pb(Mg1/3Nb2/3)O3 (PMN) into PTmN to form two Yuan (1-x) PTmN-xPMN solid solution ceramics. The XRD pattern shows that all the components belong to the orthogonal phase and the space group is Pbnm. [3]. To understand the origin of clover domain structure formation, Inoshita T examined the crystallographic characteristics of the ferroelectric state in YbMnO3 through a transmission electron microscope. The interesting feature based on the ferroelectric state is that the clover domain structure with pseudo sixfold symmetry is observed in the transmission electron microscope image that the beam is incident parallel to the hexagonal axis. In this study, the experimental conditions where the electron beam is incident perpendicular to the hexagonal axis are especially used. It was found that various ferroelectric domain structures including the clover domain structure exist under current conditions [4]. Fan Z used transmission electron microscopy to fully study the domain structure in the prototype antiferroelectric perovskite PbHfO3. At the micrometer level, various antiferroelectric domain structures in PbHfO3 were observed and analyzed, including the new "shamrock pattern" domain morphology. In another prototype antiferroelectric perovskite, PbZrO3, the antiferroelectric domains seem to favor the "layered pattern" [5]. Kaut H analyzed many image segmentation techniques. It was found that most of the techniques could not be applied to complex environments, and some work was done using Markov Random Field (MRF). It was found that this model adapts well to complex environments but is designed with strict calculations. The article praises color image segmentation and neural network-based methods. At the same time, the article pays more attention to the segmentation technology of distance image and magnetic resonance image. [6]. Maninis K K proposed the Convolution Orientation Boundary (COB), which starts from the general image classification Convolutional Neural Network (CNN) to generate multi-scale directional contours and region hierarchies. COB is computationally efficient because it requires a single CNN forward pass to perform multi-scale contour detection and hierarchical segmentation on sparse

boundaries. The method is very novel, and there are qualitative breakthroughs in performance, and invisible categories and data sets can be Very generalized. In particular, we show that learning to estimate not only the contour strength but also the direction provides more accurate results. A large number of experiments were conducted on low-level applications on BSDS, PASCAL context, PASCAL segmentation and NYUD to evaluate boundary detection performance, showing that COB provides the most advanced contour and region hierarchy in all data sets [7]. Zhang K established a new segmentation method for uneven intensity images. Non-uniform samples must have Gaussian distributions with different mean and variance. Through image mapping, the image in another area is still Gaussian, but the image difference is obvious. At this time, if the bias field is multiplied by the original image signal, the median value of the Gaussian distribution in the adaptive transformation area can be calculated. In the entire imaging area, the maximum authenticity of the energy function is clear, which is a piecewise constant function [8]. Experts and scholars at home and abroad have conducted detailed research on ferroelectric domain structure and image segmentation technology, but there are still shortcomings in the combination of the two fields, and there are few related research designs.In this paper, the piezoelectric force microscope is used to detect the nanoscale ferroelectric domain structure, and the image segmentation technology is used to study image distortion related factors. After repeated experiments and clear redundant data, the factors affecting image distortion are found, which reduces the probability of image distortion.

2. Ferroelectric Domain Structure and Image Segmentation Method

2.1. Introduction to Ferroelectric Materials and Their Characteristics

In nature, crystals can be divided into seven main crystal systems and thirty-two points combined according to symmetry. Among them, there are 20 points that do not have central symmetry, and the electric energy moment generated by their elastic deformation will change, which is called piezoelectric body. Among the twenty points, there are ten types of points with only one crystal axis (at rest). These ten points are called poles and they are: 1, 2, i, 2ii, 4, 4ii, 3, 3i, 6 and 6ii. If the pole crystal has spontaneous polarization and can change the spontaneous polarization when the temperature changes, it is called a pyroelectric crystal. Among thermoelectric crystals, the crystal that changes the direction of spontaneous polarization under the action of an electric field is ferroelectric [9]. Its structure is shown in Figure 1:

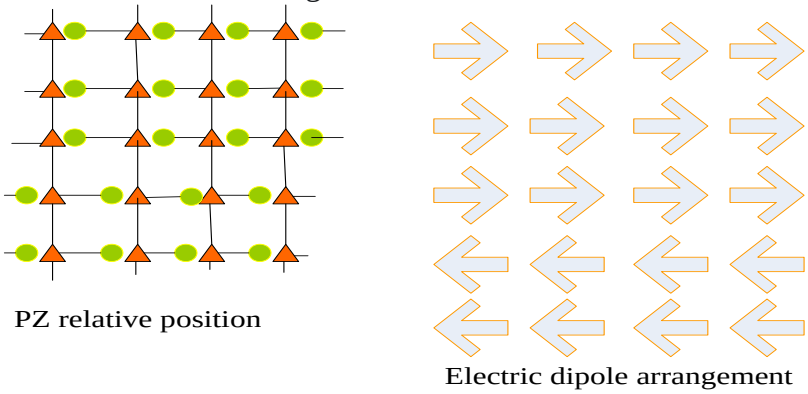

Figure 1. Ferroelectric material structure

(1) Spontaneous polarization

Ferroelectric material is a kind of dielectric material. It has spontaneous polarization in two or more directions within a certain temperature range, and its spontaneous polarization will occur with the direction and magnitude of the external field (common electric field, temperature field, etc.) When the ferroelectric is below the critical temperature, it will transform from the paraelectric phase to the ferroelectric phase. This critical temperature is the Curie temperature (TC). Above the Curie temperature, the ferroelectric material has a cubic crystal structure. At this time, the positive and negative charge centers coincide, and the ferroelectric material is in a non-polarized state, that is, the paraelectric phase; when the temperature drops below the Curie temperature, the ferroelectric material is in the unit cell The atoms move, due to the different displacements of the positive and negative ions, the positive and negative charge centers no longer overlap, resulting in an electric dipole moment. Polarization refers to the electric dipole moment per unit volume, that is, when the iron is below the Curie temperature Electrical materials exhibit ferroelectricity in a macroscopic view [10]. The thermodynamic relationship can prove that the coefficient of the positive piezoelectric effect and the coefficient of the inverse piezoelectric effect are equivalent.

For an isothermal system, the relationship between the stress, strain and electric field of the piezoelectric material can be written as:

$$G_{\mathrm{i}} = g_{ik}^{U} F_k + x_{ij} U_j,\ j = 1,2,3; i,k = 1,2,...,6 \tag{1}$$

$$X_j = x_{ij} F_i + \delta_{ih}^{F} U_h,\ j,h = 1,2,3; i = 1,2,...,6 \tag{2}$$

Among them, g_{ik}^{U} and δ_{ih}^{F} are the dielectric constant matrix of the piezoelectric material under constant stress and the elastic compliance matrix under constant electric field, respectively. Equations (1) and (2) are generally called piezoelectric constitutive equations.

If the piezoelectric stress constant u_{ji} is selected as an independent variable, the piezoelectric constitutive equations can also be expressed in another form:

$$F_j = a_{ik}^{U} G_i - x_{\mathrm{ij}} U_j,\ j = 1,2,3; i,k = 1,2,...,6 \tag{3}$$

$$X_j = \mathrm{u}_{\mathrm{ij}} G_j + \delta_{ih}^{G} U_h,\ j,h = 1,2,3; i = 1,2,...,6 \tag{4}$$

Among them, a_{ik}^{U} and δ_{ih}^{G} are the dielectric constant matrix under constant strain and the elastic stiffness matrix under constant electric field respectively. u_{ij} is the matrix of piezoelectric stress coefficients. The above two sets of piezoelectric constitutive equations are essentially the same. The piezoelectric strain coefficient matrix x_{jh} and the piezoelectric stress coefficient matrix u_{ij} can be converted mutually:

$$x_{ij} = u_{jk} g_{ik}^{U},\ j = 1,2,3; i,k = 1,2,...,6 \tag{5}$$

(2) Dielectricity

Under the influence of the external electric field, the charge inside the ferroelectric will have a position deviation, so that the center charge will no longer overlap, resulting in the appearance of a dipole. The external electric field can affect the dipole to keep its polarization direction consistent with the external electric field, resulting in dielectric polarization. If a uniform dielectric is placed on both ends of a plate capacitor, under the effect of polarization, the capacitance value of the

capacitor will increase several times compared to the vacuum capacitance value. This property is expressed by dielectric [11]. Parallel plate capacitor formula

$$C = \frac{\lambda_1 \lambda_2 B}{l} \tag{6}$$

Where λ_1 is the vacuum dielectric constant; λ_2 is the dielectric constant to be calculated; l is the distance between the parallel plates (m); B is the relative area of the two parallel plates. When the relative area of the parallel plates of the two parallel plate capacitors is equal to the distance between the parallel plates, when the medium is full, the capacitance is C; when there is a vacuum between the plates, the capacitance C_Z is obtained by formula 10:

$$\lambda_2 = \frac{C}{C_Z} \tag{7}$$

Formulas (9) and (10) can be constructed. When the dielectric between the two laminates is empty, the plate capacitor will increase its capacity, and the relative dielectric constant can be described by increasing the capacity. The relative permittivity is a number greater than one. The relative permittivity can be abbreviated as the permittivity.

(3) Pyroelectricity

The pyroelectric effect [12] refers to the phenomenon that when the temperature changes, the charge center inside the crystal deviates from the original position, which causes the spontaneous polarization of the material to also change, which makes the two ends of the crystal appear different bound charges.

2.2. Introduction to Ferroelectric Domains

Inside the ferroelectric material, the dipole moments of different unit cells are different, and adjacent unit cells tend to form the same polarization direction. Eventually, a small area with the same polarization direction will be formed inside the material, which is called the electric domain. The area between the electrical domain and the electrical domain is called the domain wall [13]. The electrical domain and the interface between the electrical domains are shown in Figure 2.

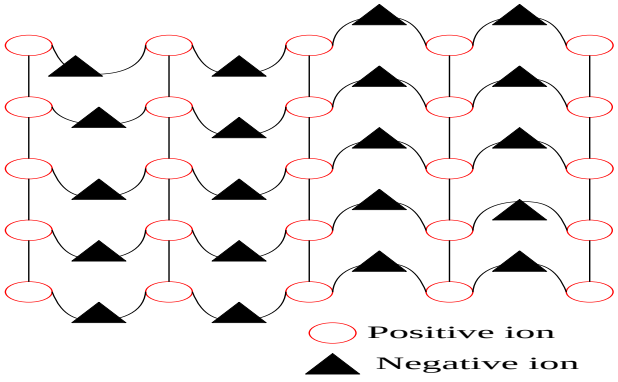

Figure 2. Schematic diagram of ferroelectric domain structure

2.3. Introduction to Piezoelectric Microscope

Piezoelectric force microscope (PFM), as shown in Figure 3, is an extended mode based on AFM

(Atomic Force Microscope) [14]. Through PFM, we can not only obtain nano-level topographic features of the sample surface, but also obtain information about the sample. The ferroelectric voltage and electric information of the sample, such as the structure of the ferroelectric domain of the sample, the polarization inversion of the ferroelectric domain, etc. The principle is to use a conductive probe instead of an ordinary probe on the basis of an atomic force microscope, and use the AC voltage generated by the signal generator to act on the sample, thereby applying an external excitation electric field on the sample, due to the inverse piezoelectric effect., The sample will produce a slight deformation and be measured by the microscope. Usually the deformation is very small (of the magnitude of pm). In order to effectively extract this signal, a lock-in amplifier is installed in the PFM. In addition, in order to obtain the maximum sensitivity of the test, it is necessary to find the vibration frequency of the probe, and then apply an identical Frequency of the external voltage, so that it reaches resonance, and in the case of resonance, the deformation of the probe can reach the maximum.

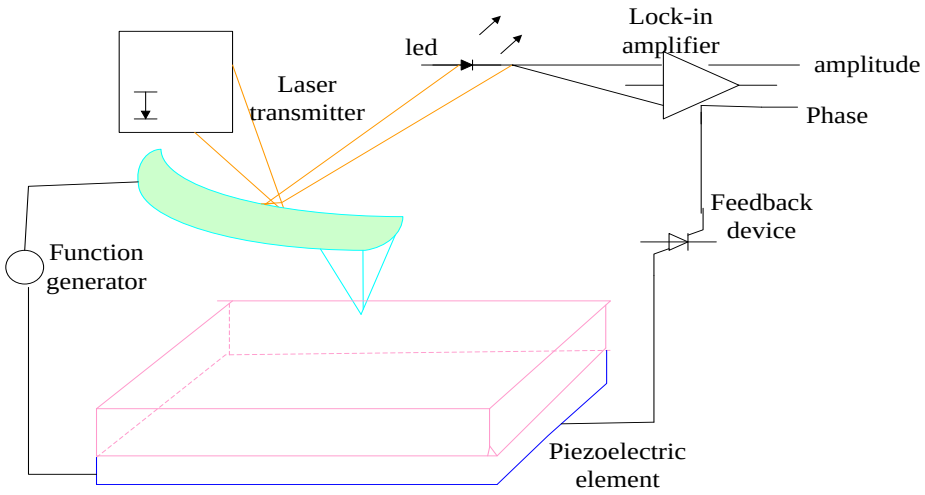

Figure 3. Basic structure of piezoelectric force microscope

In the PFM test, the voltage applied to the needle tip can be divided into two parts: DC and AC. When the image is scanned, the DC voltage is 0, and when the hysteresis loop test is performed on the local points, it is necessary to apply a DC polarization voltage while applying the AC voltage. So the voltage actually applied to the needle tip can be expressed as:

$$U_T = U_Z + U_J \cos(ft) \tag{8}$$

Among them, U_T is the voltage at the tip of the needle, U_Z is the applied DC voltage, U_J is the extreme value of the AC voltage, and f is the frequency of the AC voltage. The response of the probe cantilever to the spatial displacement mainly reflects the piezoelectric response of the test sample under the action of an electric field, and its value can be obtained by the following simple relationship:

$$B = Ye_x U_J \tag{9}$$

Where B is the collected vibration amplitude, Y is the gain coefficient provided by the instrument, e_x is the piezoelectric coefficient of the test sample, and U_J is the AC voltage applied to the needle tip.

Because PFM images are mainly used in high-tech fields, there are certain requirements for the accuracy of the images, but PFM lacks information feedback in nano-operations, and cannot display real-time operation results. Only after the operation is re-imaging can the operation results be obtained. PFM operation requires high-resolution observation and high-precision operation of the area of interest with the help of probes, but because the probe driver is nonlinear and there are factors such as system temperature drift, the observer will be inaccurate when observing. This seriously hinders the effective progress of PFM nanometer observations, so the positioning problem of the probe in the task space has become a problem that hinders the wide application of PFM, where the linearity of the driver, the system temperature drift and the probe tip broadening effect are the solutions. Scan driver PZT non-linearity refers to the phenomenon that the voltage on the driver is constant, but the displacement changes slowly with time, and finally becomes stable. At present, there are effective methods to solve the PZT nonlinear problem of the scan driver at home and abroad, so the PZT nonlinear problem is no longer studied in this research [15].

The temperature drift of the system refers to the relative random drift between the probe and the measured object due to the relative random drift of the PZL tube and other parts of the system during the PFM imaging process at the ambient temperature, which causes the scanned image to fail to truly reflect the true object of the target. Because this kind of change is difficult to control in real time to eliminate the influence of system temperature drift, the image obtained by PFM scanning has a certain degree of distortion, which seriously reduces the accuracy of the PFM image and makes the scanned image inconsistent with the scanned sample. When PFM scans the image, due to the probe tip broadening effect, it will seriously affect the quality of the PFM scanned image, and increase the impact of uncertain factors on the probe positioning and PFM image accuracy during the nano-operation. The probe tip broadening effect refers to the inaccuracy of the image formed by the scan due to the specific topography of the probe tip during the scanning process due to the topography of the probe tip during the scanning process. Compared with the actual shape of the sample, it is too "wide", which leads to a decrease in the accuracy of the scanned image. The above problems are currently the main problems affecting the accuracy of PFM images. If the above problems cannot be effectively solved, the use of distorted PFM images for scientific research and nanoscale device processing and manufacturing will severely restrict the development of nanotechnology due to inaccurate measurement and operation., Limiting the wide application of PFM in the nano-scale field [16].

2.4. Image Segmentation Technology

Image segmentation [17] can be said to be an old and novel topic in the computer field. It is said that it is old because of the rise of computers. Scholars have begun to study and discuss him, saying that he is novel because of His discussion has not stopped so far, and researchers are constantly studying new methods to make the results of segmentation more ideal. Image segmentation is to combine

A process of extracting the part that people are interested in. People usually call the part of interest as the foreground (Q), and they are not interested.

The part is called background (B). The mathematical definition of image segmentation is as follows:

Let I denote an image, and the process of dividing I into m sub-regions is called $\{I_1, I_2, I_3, ..., I_m\}$ -segmentation. The conditions that are satisfied are as follows:

$$P_{x=1}^{m} I_x = I \tag{10}$$

Among them, I_x is a connected domain, x=1,2,3,...,m.

$$I_x \mathrm{I}\ I_y = \emptyset, \mathrm{x} \neq \mathrm{y} \tag{11}$$

$$W(I_x) = TRUE \tag{12}$$

$$W(I_x \mathrm{Y}\, I_y) = FALSE \tag{13}$$

For any adjacent pixels $I_x and I_y$, where $W(I_x)$ is a logical predicate defined on the point of set I_x, and ∅ represents an empty set.

With the rapid development of science and technology in recent years, the types and quantities of images are wide, and specific segmentation methods must be used for specific images. No method is omnipotent. Different segmentation methods can only be applied to one or several Kind of image. Below we introduce some specific image segmentation methods. In general, we summarize the method of image segmentation as: threshold-based segmentation

Cutting method, edge-based segmentation method, region-based segmentation method [18], its structure is shown in Figure 4.

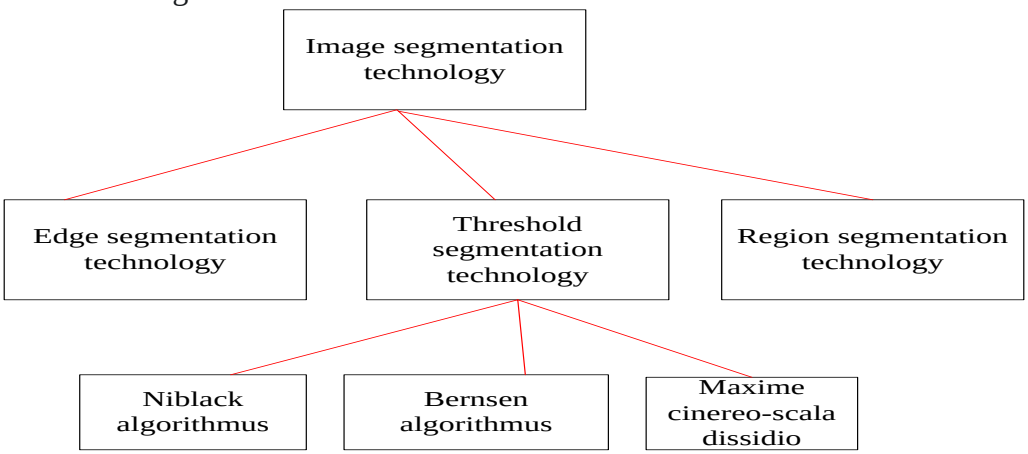

Figure 4. Image segmentation technology division

(1) Segmentation method based on threshold

Threshold segmentation is the simplest clustering segmentation algorithm. It traverses all pixels and compares the value of a single pixel with a fixed threshold to obtain the result of the previous background segmentation. The most widely studied method of this type is the Maximum Between-Class Variance Method (otsu) [19], which implements image segmentation by calculating the maximum gray-scale variance between different classes. The simplest example is to use otsu to implement image segmentation. In an image including target, background and noise, a certain threshold Q is selected to divide the image into two parts: the part larger than Q and the part smaller than Q.

$$I(m,n) = \begin{cases} 1, f(m,n) \rangle Q \\ 0, f(m,n) \langle Q \end{cases} \tag{14}$$

For more complex images, the global single threshold often cannot get the ideal clustering effect,

and the local multi-threshold segmentation method developed from this. Compared with the global threshold, the local threshold can better preserve the image details. By setting different segmentation thresholds for different regions of the image, the image segmentation can be made more delicate, and more cognitive target areas of the image can be retained. Because multiple thresholds are used to separate different image regions independently, the color information will jump at the junction of the two thresholds. In order to eliminate this intuitive color jump, the jump boundary can be smoothed. Common local threshold methods include Niblack algorithm, Bernsen algorithm and so on.

$$I(m,n)=\begin{cases} j, & f(m,n)\rangle Q_2 \\ k, Q_1\langle f(m,n)\le Q_2 \\ l, & f(m,n)\le Q_1 \end{cases} \tag{15}$$

(2) Edge segmentation

In graphic imaging, the edge intensity of the image (ie, the gradient of the image) is usually used to characterize the sharpness of the image. Generally speaking, the edge of a grayscale image generally refers to an area where the grayscale of the image changes drastically. These changes are often caused by the shape of the object, the exposure of external light, and the reflection of light on the surface of the object. For the same field of view, the stronger the edge of the image, the clearer the image. Commonly used edge detection operators can be divided into first-order differential edge operators and second-order differential edge operators. Among them, the first-order differential operators mainly include Roberts operator, Prewitt operator, Krisch operator and Sobel operator. The difference between these first-order differential operators is that the calculation templates used to calculate the horizontal and vertical differential components of the image are different. The second-order differential operators mainly include Laplace operator and LOG operator.

Roberts operator [20] is as described in formula (16), and this algorithm is mainly used for edge detection on a plane.

$$I(m,n)=\sqrt{f(m,n)-f(m+1,n+1)^2+\left(f(m+1,n)-f(m,n+1)\right)^2} \tag{16}$$

Sobel operator, as shown in formula (17), is mainly used to detect the gradient change of the operator.

$$I(m,n)=\sqrt{A_c^2+B_d^2} \tag{17}$$

$$\begin{aligned} A_c &= \{f(c+1,d-1)+2f(c+1,d)+f(c+1,d+1)\} \\ &-\{f(c-1,d-1)+2f(c-1,d)+f(c-1,d+1)\} \end{aligned} \tag{18}$$

$$\begin{aligned} B_d &= \{f(c-1,d+1)+2f(c,d+1)+f(c+1,d+1)\} \\ &-\{f(c-1,d-1)+2f(c,d-1)+f(c+1,d-1)\} \end{aligned} \tag{19}$$

(3) Regional segmentation

The region segmentation method uses the spatial information and gray information of the image to divide the target into different regions. The region segmentation algorithm [21] does not have the problem of discontinuous boundaries, but it is sensitive to the selection of initial points and can easily lead to local optimal conditions. There are generally two regions-based image segmentation methods, the first region grows, and the second region splits and merges. Region growth is

artificially given several seed points in advance. After the seed points are obtained, we give certain rules to make the pixels around the seed points merge into a new seed point under the premise of satisfying this rule, and then repeat this Process until the pixels around the seed point no longer meet this rule. The region growing algorithm generally includes 3 steps.

(1) Choose a suitable growth point.

(2) Determine the similarity criterion, namely the growth criterion.

(3) Determine the growth stop condition.

Generally, when all the pixels in the image are allocated, the growth stops. Region growth is a process from micro to macro, that is, from pixels to regions. Region splitting and merging is a process from macro to micro to macro, that is, the image is first divided into several large regions, and then these large regions are split according to certain criteria, until it can no longer be split. The divided small areas are then merged with the surrounding areas with the same characteristics using certain criteria, and the final result is the result of the segmentation.

2.5. Segmentation Evaluation Index

This article briefly introduces three methods to evaluate the relevant indicators of image segmentation:

1. Segmentation accuracy

The segmentation accuracy [22] is the percentage of the accurate segmentation area to the standard segmentation result. Normally, standard segmentation is the result of expert hand-drawn. The mathematical definition of segmentation accuracy is as follows:

$$SA = \left(1 - \frac{|C_M - R_M|}{C_M}\right) \times 100\% \tag{20}$$

Among them, C_M represents the reference area of the segmented image manually drawn by the expert, R_M represents the real area of the image obtained by the algorithm segmentation, and $|C_M - R_M|$ represents the number of pixels that are incorrectly segmented.

2. Over-segmentation rate

The over-segmentation rate [23] is the ratio of the number of pixels outside the reference result of the algorithm segmentation result, and its mathematical definition is as follows:

$$OR = \frac{Y_M}{C_M + Y_M} \tag{21}$$

Among them, Y_M represents the number of pixels whose segmentation result is outside the reference result.

3. Under-segmentation rate

The under-segmentation rate [24] is the ratio of the pixel points that the result of the algorithm segmentation is not in the reference result, and its mathematical definition is as follows:

$$UR = \frac{Z_M}{C_M + Y_M} \tag{22}$$

Among them, it indicates the number of pixels that the result of algorithm segmentation is not in

the reference result.

3. Experiment and Analysis

The PFM experiments in this chapter are all carried out on the Bruker Icon AFM system. The conductive AFM probe used in the experiment is the HQ:NSC19/Cr-Au probe plated with chromium-gold on the surface. Using the energy equalization method, the elastic stiffness coefficient of the probe can be determined to be 1.6 N/m. The sample is a periodically polarized LiNbO3 single crystal with a thickness of 0.5 mm. In order to facilitate subsequent analysis, we set the coordinate system as follows: the x-axis is perpendicular to the domain wall, x=0 is set on the domain wall under study, and the z-axis is perpendicular to the upper surface of the sample. For PFM imaging, the pre-pressure of the probe to the sample is set to ~30 nN. Adjust the position of the cantilever wall of the probe so that the incident point of the laser is directly above the probe.

In this chapter, in PFM imaging, select a working frequency far lower than resonance. Here we choose 20 kHz, which is much lower than the actual resonance frequency ~350 kHz. The amplitude of the alternating excitation voltage is 5 V. When the PFM is performing the scanning action, the relative displacement of the probe and the substrate is caused by the temperature change of the PFM system, and the actual position of the scanned image at intervals is also displaced due to the influence of the expansion coefficient of each part of the instrument. T The temperature drift compensation method based on partial scanning, its principle is to set the feature points in the scanned image as markers, and use the partial scanning method to obtain the change of the position of the markers, so as to monitor the temperature drift of the system, and then compensate the temperature drift displacement to In real-time operation, to achieve the purpose of temperature drift compensation [25]. Use the current relatively well-formed probe modeling method for image reconstruction, and use the blind modeling algorithm to improve the probe modeling method [26].

The VPFM and LPFM images obtained by PFM scanning are shown in Figure 5. The response data of VPFM and LPFM comes from two independent lock-in amplifiers. Each lock-in amplifier generates two sets of data: a set of in-phase response data (real part: Real) and a set of out-of-phase data with a 90 ° phase lag (imaginary part). : Imaginary). These two sets of data can be further converted into amplitude and phase angle. The latter is the way PFM data is presented in most literature. In order to facilitate the quantitative analysis of PFM data, the original in-phase and out-of-phase data are still used here. First extract the PFM piezoelectric response curve in Figure 5.

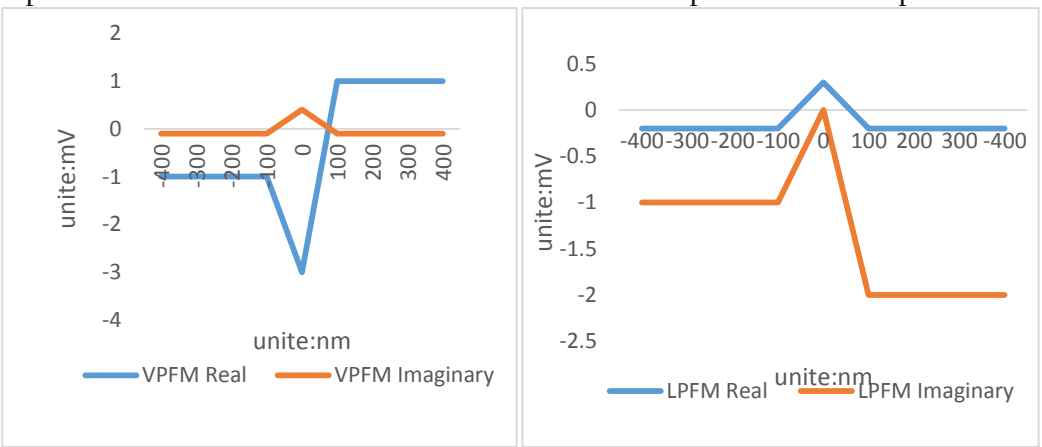

Figure 5. PFM responds to in-phase and out-of-phase data

For this 180 ° domain structure, since the piezoelectric response curve corresponding to each PFM line scan is essentially the same, we can average all the line scans to enhance the signal-to-noise ratio of the data. The result is shown in Figure 6.

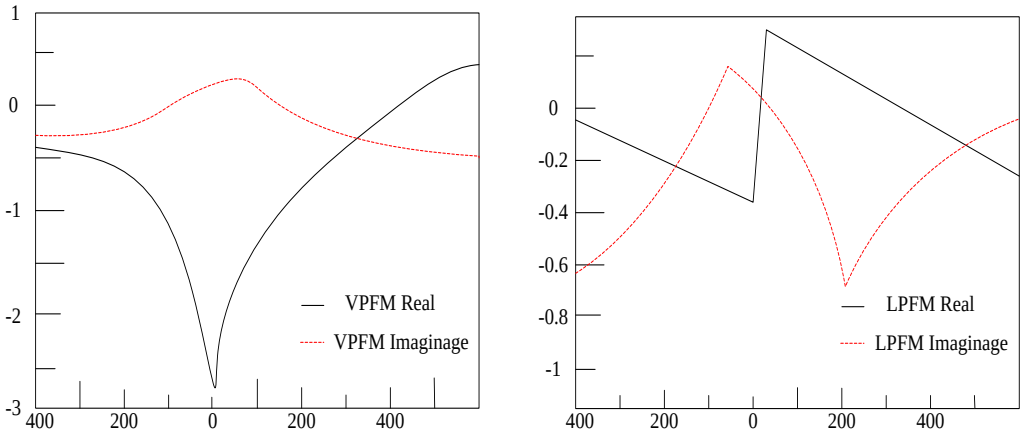

Figure 6. PFM piezoelectric response curves in the same phase and out of phase

What needs to be explained here is that the VPFM and LPFM response curves shown in Figure 6 both have large background noise. This has been noticed by Jungk et al. in their early VPFM imaging work. In order to facilitate the study of the behavior of background noise, they first thought of mapping the real and imaginary signals obtained from the VPFM imaging data onto the complex plane. For VPFM imaging of LiNbO3 single crystal +z domain and –z domain, the expected value of the VPFM phase difference under ideal conditions is 180 °, and the amplitude is the same [27-28].

However, the VPFM response obtained by the actual experiment is usually not consistent with the ideal situation, and is related to the actual PFM alternating voltage driving frequency. This is caused by the background noise of the imaging system. It should be noted that although the amplitude and phase angle of the background noise of the VPFM response are different at different frequencies, the intrinsic contrast amplitude 2d of the 180 ° twin domain is the same. Next, we need to map the PFM signal after background noise processing on the complex plane back to the scan coordinate space to obtain the relationship between the PFM piezoelectric response and the domain wall. Comparing the data related to the original scan curve, we can find a very important feature [29]: The imaginary signal of PFM is almost zero. This means that the effective information of PFM imaging is compressed into one channel after background noise processing, facilitating further research on the quantitative characterization of PFM.

In order to further verify the effectiveness of the algorithm, starting from the image segmentation results, we will compare the original picture and the image segmentation algorithm. We select multiple images for segmentation. The average value obtained by comparing the evaluation index calculation formula includes the error segmentation rate and over segmentation. Rate, under-segmentation rate and accuracy rate, the results are shown in Table 1.

Comparing the data in Table 1, we can draw the following conclusion: each algorithm has obvious advantages for image segmentation. It performs well in terms of mis-segmentation rate, over-segmentation rate, under-segmentation rate, and accuracy, and presents a good image segmentation effect, but Threshold-based image segmentation technology performs well in all aspects, and edge segmentation technology performs slightly inferior in mis-segmentation rate and

accuracy. The overall advantages of regional segmentation are more balanced.

Table 1. Image segmentation evaluation index

	Split rate	Over-segmentation rate	Under-segmentation rate	Accuracy
Threshold segmentation	0.06	0.03	0.07	0.943
Edge segmentation	0.32	0.07	0.08	0.889
Region segmentation	0.13	0.15	0.07	0.933

Table 2. Comparison of image segmentation efficiency and accuracy

	Threshold segmentation	Edge segmentation	Region segmentation
Split time	0.986	1.311	0.967
Segmentation accuracy	0.912	0.925	0.903
Segmentation efficiency	0.965	0.941	0.976

Comparing the data in Table 2, each algorithm performs well in response time and accuracy. In general, the overall data of the threshold segmentation technology is more balanced, the edge segmentation response time is longer, and the efficiency is lower, but its accuracy is higher, and the region segmentation response time Shorter and more efficient, but slightly inferior in accuracy.

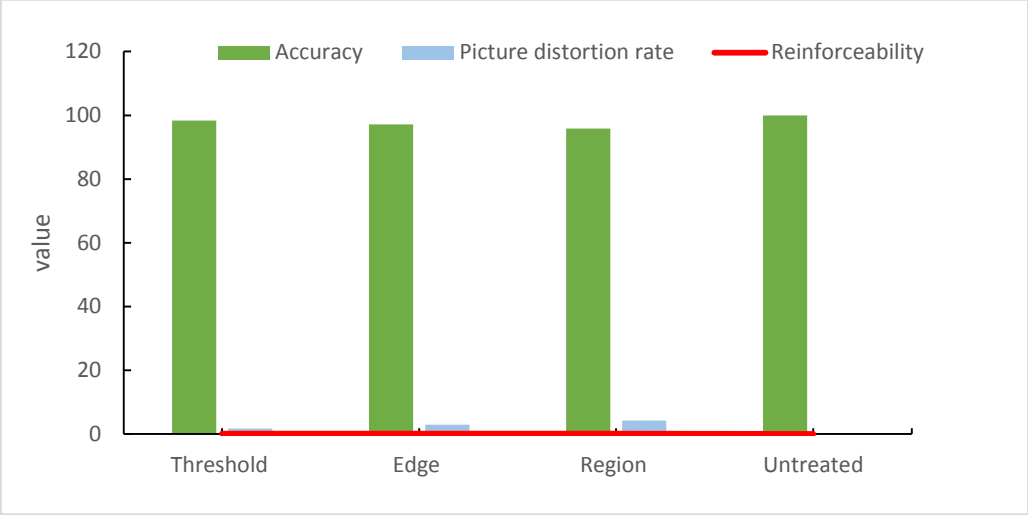

Figure 7. Evaluation and optimization of the effect of each image segmentation technology

Comparing the data in Figure 7, the image rendering effect of each image segmentation algorithm is not much different, but in terms of image distortion, compared with the original image, threshold segmentation and region segmentation perform poorly, and there is much room for improvement. Generally speaking, the distortion of the overall image is not high, and the detail retention is good.

4. Discussions

In this paper, the piezoelectric force microscope is used to detect the structure of the nano-scale

ferroelectric domain. After reducing the unfavorable imaging factors detected by the PFM microscope, the relevant structure image of the ferroelectric domain is obtained, and then the image is segmented. The image segmentation technology found that each technology performs well in terms of image distortion, but the edge segmentation technology retains better details. The various evaluation indicators of threshold segmentation technology are more balanced. In terms of specific applications, the edge image segmentation technology can be used to retain most of the details of the image, and then the threshold segmentation technology can be used to evaluate the image as a whole for better observation and research.

5. Conclusion

Image segmentation is an important branch in the image processing process. It is designed for extracting objects of interest. It can separate redundant information or extract object contours for the next stage of processing. The first part is that image analysis and processing must rely on image segmentation. After segmentation, there is an opportunity to directly process the target to reduce the workload. At the same time, it is also convenient for us to measure and calculate the target, which is very important for the development of image feature extraction, image matching, target recognition and other fields. Image segmentation is of great significance and has a wide range of application scenarios. But in actual application, it still faces many challenges. Such as imaging equipment, shooting methods, external interference and picture quality all affect image segmentation. Especially complex backgrounds test the technology of image segmentation. Even if it is the same image, but the research purpose is different and the research object is different, the difficulty of segmentation is also different. This brings trouble to image segmentation. Although there are many image segmentation methods in theory, the general method is not suitable for all objects [30]. Looking forward to improving the image segmentation technology in the future to improve the accuracy and precision of the image and reduce the distortion of the image.

Funding

This article is not supported by any foundation.

Data Availability

Data sharing is not applicable to this article as no new data were created or analysed in this study.

Conflict of Interest

The author states that this article has no conflict of interest.

References

[1] Lambeck P V, Jonker G H. The nature of domain stabilization in ferroelectric perovskites. Journal of Physics & Chemistry of Solids, 2017, 47(5):453-461.

[2] Katayama K, Shimizu T, Sakata O, et al. Orientation control and domain structure analysis of {100-oriented epitaxial ferroelectric orthorhombic HfO2-based thin films. Journal of Applied Physics, 2016, 119(13):102903. https://doi.org/10.1063/1.4945029

[3] A J J W, A Y W, B J I, et al. Tunable thermal conductivity via domain structure engineering in ferroelectric thin films: A phase-field simulation - ScienceDirect. Acta Materialia, 2016, 111:220-231.

[4] Wang Z, He C, Qiao H, et al. In Situ Di, Piezo, Ferroelectric Propertiesand Domain Configurations of Pb(Sc1/2Nb1/2)O3–Pb(Mg1/3Nb2/3)O3–PbTiO3 Ferroelectric Crystals. Crystal Growth & Design, 2017, 18(1):145-151. https://doi.org/10.1021/acs.cgd.7b01023

[5] Fan Z, Ma T, Wei J, et al. TEM investigation of the domain structure in PbHfO3 and PbZrO3 antiferroelectric perovskites. Journal of Materials Science, 2020, 55(12):4953-4961. https://doi.org/10.1007/s10853-020-04361-8

[6]Kaut H, Singh R. A Review on Image Segmentation Techniques for Future Research Study. International Journal of Engineering Trends and Technology, 2016, 35(11):504-505.

[7]Maninis K K, Pont-Tuset J, Arbelaez P, et al. Convolutional Oriented Boundaries: From Image Segmentation to High-Level Tasks. IEEE Transactions on Pattern Analysis & Machine Intelligence, 2017, PP(99):1-1.

[8] Zhang K, Zhang L, Lam K M, et al. A Level Set Approach to Image Segmentation With Intensity Inhomogeneity.. IEEE Transactions on Cybernetics, 2017, 46(2):546-557. https://doi.org/10.1109/TCYB.2015.2409119

[9]Jiang Zhaoxiu, Wang Yonggang, Nie Hengchang, et al. The effect of polarization state and direction on the domain transition and phase transition behavior of Pb(ZrTi)O ferroelectric ceramics under uniaxial compression. Acta Phys. Sin, 2017, 66(2):209-216. https://doi.org/10.7498/aps.66.024601

[10]CHEN Yu, HU Chi, XU Qian, et al. Research progress in micro-domain change mechanics of ferroelectric materials. Materials for Mechanical Engineering, 2019, 043(006):64-71.

[11]Chen Yu, Zhou Huajiang, Xie Shaoxiong, et al. Fatigue failure behavior of ferroelectric materials. Advances in Mechanics, 2021, 51(4):1-37.

[12]Zhang Yangjun, Wang Bingqin, Zhou Yichun. Domain switching model of the nonlinear behavior of ferroelectric thin films under multi-field coupling. Journal of Vacuum Science and Technology, 2018, 38(04):68-71.

[13] Zhang Lixue, Ren Xiaobing. Aging effect and super-large recoverable electro-induced strain of ferroelectric materials. Progress in Materials in China, 2016, 35(006): 442-448.

[14] Liu Di, Wang Jing, Wang Junsheng, et al. Phase-field simulation of strain control PbZr_((1–x))Ti_xO_3 film micro-domain structure and macro-ferroelectric properties. Acta Phys. Sin, 2020, v.69(12)): 201-210. https://doi.org/10.7498/aps.69.20200310

[15] Huang Fang. Research on Image Segmentation Method. Journal of Chifeng University (Nature Edition), 2016, 32(021): 20-21.

[16] Geng Yanping, Guo Xiaoying, Wang Huaxia, et al. MR brain image segmentation algorithm based on wavelet image fusion algorithm and improved FCM clustering. Computer Science, 2017, 44(012):260-265.

[17]Zhang Yupei. Research on image segmentation technology based on partial differential equations. Times Agricultural Machinery, 2017, 000(009): 114-114.

[18]Dong Xinyu, Chen Hanyue, Li Jiaguo, et al. Unsupervised color image segmentation based on multi-method fusion. Journal of Shandong University (Engineering and Technology Edition), 2019, 49(2):64-69.

[19]Yang Haiping, Ming Dongping. High-resolution image segmentation based on multi-layer optimal scale. Journal of Geo-Information Science, 2016, 18(5):632-638.

[20]He Zhendong, Wang Yaonan, Liu Jie, et al. Image segmentation of high-speed rail surface

defects based on background difference. Chinese Journal of Scientific Instrument, 2016, 037(003): 640-649.

[21] Dai Shan, Li Guangjun. Adaptive image segmentation combined with nearest neighbor propagation clustering. Computer Science, 2016, 043(0z1):191-193.

[22] He Fuliang, Guo Yongcai, Gao Chao, et al. Image segmentation of mature mulberry based on visual saliency and pulse coupled neural network. Transactions of the Chinese Society of Agricultural Engineering, 2017, 33(006): 148-155.

[23] Zhang Yifan, Kang Yan, Lin Ying. Improved watershed image segmentation algorithm. Electronic Technology and Software Engineering, 2016, No.75(01):109-109.

[24] Zhao Lichuan, Gao Yang. Medical image segmentation algorithm based on improved self-affine mapping system and parameter active contour. Journal of Computer Application Research, 2017, 34(002):616-620.

[25] Han Hao, Zhan Ke, Wang Xianying, et al. The effect of annealing time on the microstructure and piezoelectric properties of BNT-BT6 films. Materials Review, 2016, v.30(06):6-10.

[26] Leng Senlin, Zeng Huarong, Zhao Kunyu, et al. Nano-piezoelectric-acoustic-thermal microscopy and its application research. Chinese Ceramics, 2017, 053(004): 38-45.

[27] Zhang Chi, Guo Jiansheng, Zhang Zhi. Preparation of Zinc Oxide Nanorods Piezoelectric Power Generation Textiles. Synthetic Fiber, 2016, 45(005): 28-31.

[28] He Shuangci, Zhong Zhicheng, Wang Jingyang, et al. The influence of substrate temperature on the optical and electrical properties of AZO thin films prepared by co-sputtering. Piezoelectric & Acousto-Optic, 2018, 40(005):784-788.

[29] He Jian, Wang Erwei, Chou Jianshe. Design and research of piezoelectric cross-type MEMS vector bionic hydrophone. Piezoelectric and Acousto-Optic, 2017, 39(002):239-242.

[30] Wang Xiaochen, Pan Rong. Adaptive image quality evaluation method based on image distortion type. Television Technology, 2016, 40(002):137-140.